We are IntechOpen, the world's leading publisher of Open Access books Built by scientists, for scientists

4,800
Open access books available

122,000
International authors and editors

135M
Downloads

Our authors are among the

154
Countries delivered to

TOP 1%
most cited scientists

12.2%
Contributors from top 500 universities

CLARIVATE ANALYTICS BOOK CITATION INDEX INDEXED

WEB OF SCIENCE™

Selection of our books indexed in the Book Citation Index in Web of Science™ Core Collection (BKCI)

Interested in publishing with us?
Contact book.department@intechopen.com

Numbers displayed above are based on latest data collected.
For more information visit www.intechopen.com

Chapter 5

Spin Average Supercompound Ultrasonography

Tsuicheng D. Chiu, Sonia Contreras and Martin Fox

Additional information is available at the end of the chapter

http://dx.doi.org/10.5772/53238

1. Introduction

Introduced to the medical field in the 1950s, ultrasound has applications across the spectrum of modern medicine including cardiology, urology, obstetrics, gynecology and abdominal imaging (kidneys, liver, spleen, gallbladder and pancreas excluding stomach and intestines which contain of air which blocks ultrasound). Vascular imaging is used especially for large vessels like the aorta. Ultrasound is also used as a guide in surgeries.

Although ultrasound is real-time, non-invasive, highly cost-effective [1], portable and uses non-ionizing radiation, its benefits are offset by penetration and resolution limitations. As a result, it has been coexists with computed tomography (CT) and magnetic resonance imaging (MRI) [2, 3]

The main goal of this research is to improve the quality and the usefulness of the ultrasound image. We present a supercompounding technique [4] which can be described as a two-dimensional spin average method. The supercompounding technique is one kind of spatial compounding. Unlike conventional compounding which typically uses a 30 degrees to 60 degrees compounding range, our spatial compounding technique which we have termed "supercompounding" uses a B-mode array that rotates around a target in a range of 120 degrees or greater. The experiments in the research use complete 360 degrees scanning to optimize results. We find that the quality of the ultrasound images is improved and whether the use of the ultrasound imaging can be extended to other applications. Our results suggest that, this technique will extend the limits of ultrasound imaging while preserving all its current benefits.

1.1. Ultrasound imaging system

The imaging system used in this research is the GE RT-3200 ultrasound imager, a relatively primitive early generation two-dimensional imager compared to modern equipment. The ba-

sic principles of commercial ultrasound are pitch and catch. The ultrasound waves are typically transmitted and received by transducers. In medical applications, reflection systems are virtually universal due to the ease of use of hand-held transducer. Such pulse-echo systems catch the reflected ultrasound waves and only one transducer is needed. Ultrasound waves are sent to an object and reflected with time delay between the transmission of the beams and the arrival of the reflected signals. All objects are taken with either a linear 7.5 MHz or a curvilinear 3.5MHz transducer. Although the GE RT-3200 is an early generation ultrasound imaging system, the results in the r should be evaluated with respect to the degree of image improvement. It is because the supercompounded image is integrated from hundreds of raw ultrasound images. If the quality of raw images is improved by modern equipments, with better compounding materials, it can result in an even better supercompounded images.

1.2. Types of ultrasound artifacts

Compared with CT and MRI, ultrasound images have lower signal-to-noise ratio because ultrasound waves are highly distorted when traveling through the tissues. The ultrasound image is constructed from the interactions between the transmitted ultrasound waves and the imaged tissues. Once the reflected ultrasound waves are distorted or compromised, the resultant image will incur artifacts that either omit or add erroneous information.

The following list states artifacts occurred in the experiments in this research and Figure 1 shows how they appear on the clinical ultrasound image.

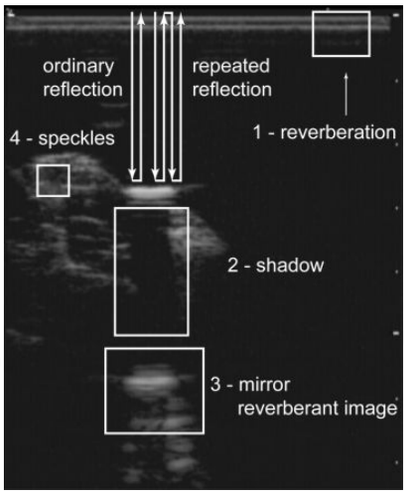

Figure 1. Artifacts: The object is a dissected rat thigh tightened with a supported wood stick placed in water bath and the image is taken using the 7.5 MHz linear transducer. Region 1 shows the reverberations, the reverberations are caused by the mismatched impedances between the wall of the water container (assembled by four 5 millimeters thick acrylic plates) and waters. Region 2 shows the shadow behind a side wall of the supported wood stick. Since the wood material is highly reflective, the stick blocks all ultrasound waves and it results the shadow. Region 3 shows a mirror reverberant image. It usually happens when a high reflective object is imaged. The reflected ultrasound waves are reflected again by the surface of the transducer and it makes the same ultrasound beams travel twice distance but with the same results. Therefore, the same or similar structures lies at the twice depth on the image. Region 4 shows speckles which come from the scattered ultrasound waves.

- Reverberation: Reverberations are multiple lines behind the physical objects normally found on the boundaries between two media, especially when the acoustic impedances of two materials are significantly mismatched as shown in Figure 2. The first and the second reflections represent the superficial and the deep boundaries of the second medium. The third to the n^{th} reflections are the reverberations coming from the trapped ultrasound waves in the second medium. The fraction of the ultrasound waves that is reflected depends on the reflection coefficient between the two media.
- Shadows: Three scenarios cause shadows on ultrasound images. Shadows are caused either by a large impedance mismatch, a highly angled boundary or a highly absorptive material.

Unlike reverberations, where only parts of the ultrasound waves can penetrate through the boundaries and are trapped in the second medium, all the ultrasound waves can be totally blocked due to an even greater impedance mismatch. Since no waves penetrate the second medium, there is no information returning from the area behind the high reflective objects.

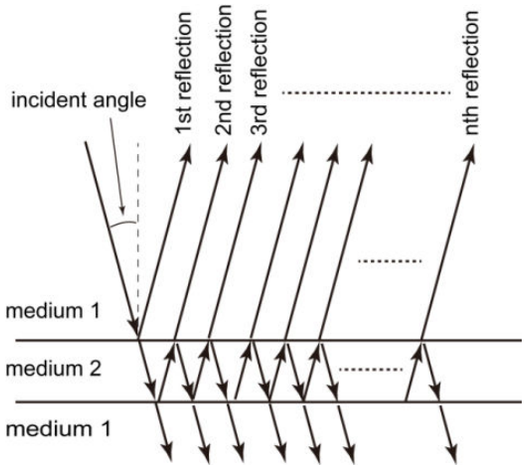

Figure 2. Illustration of reverberations. Reverberations show as multiple lines as the ultrasound waves bounce back and forth in the second medium, resulting from the mismatched impedances between the medium 1 and 2.

Acoustic absorptive materials can cause the shadowing effect for another reason. If ultrasound waves are totally absorbed by the target material, shadows will also result because no waves return to the transducer.

The third scenario is caused by the shape, not the material of the object. As illustrated in Figure 1, the incident ultrasound waves contact the boundaries and the reflected waves bounce back to the transducer. When the incident angle is large enough, the reflected ultrasound waves are not reflected back to the transducer. Large incident angle scan cause low intensities (parts of the reflected waves going back to the transducer) or even shadows (all waves redirecting away from the transducer) behind the boundaries on the image.

- Mirror reverberant images: A reverberant image occurs when the same structure appears twice. When the reflected ultrasound waves return to the transducer with enough energy

to perform a second reflection on the surface of the transducer. It gives the same results with twice traveling distance for the same ultrasound waves; therefore, the ultrasound imaging systems are misled causing apparent imaging of nonexistent structures lying at the twice the depth of the original object.

- Speckles: Ideally when the ultrasound waves contact the object, the waves are either reflected or transmitted. However, small portions of the ultrasound waves can interfere coherently. The accumulation of random scatterings in the tissue volume results in intense fluctuations on the image that degrades its quality. The resultant speckle pattern can be modeled geometrically as a random walk of component phasor [6].

1.3. Point spread function

The response of an imaging device to a point object is described as a point spread function (PSF), a blurring process intrinsic to many imaging modalities. As a result, the acquired images can be convolved with a PSF. This phenomenon makes the general image function described by[7]:

$$i(x,\ y) = \iint h\,(x,\ y; \xi,\ \eta) i_r(\xi,\ \eta) d\xi d\eta \tag{1}$$

where i is the obtained image, h is a generalized PSF and $(x, y; \xi, \eta)$ are the output and input pair coordinates in input and output planes, with i_r being the spatial distribution or raw image before convolving with the PSF. The equation 1 shows a space variant PSF. The true spatial distribution is blurred by the PSF. PSFs are space variant in most ultrasound imaging systems, especially due to focusing, as illustrated in Figure 3. Since there is no closed form relationship between input and output signals, further image enhancement is difficult. In the most probable scenario, the algorithms that work at certain regions are not applicable to the whole image. Due to non-stationary PSFs, space variant algorithms have to be used. If the image has a regularized PSF, it can be expressed using the convolution operation:

$$i(x,\ y) = \iint h\,(x - \xi,\ y - \eta) i_r(\xi,\ \eta) d\xi d\eta \tag{2}$$

Space invariant algorithms can be used to improve its quality. Supercompounding provides an image with a more regularized PSF. "Regularized" implies that the lateral and axial resolutions are the same; indeed a circularly symmetric point spread function. This benefit can allow linear filtering to become more efficient and reliable and to simplify the image processing.

We propose an enhanced compounding technique which we term supercompounding. It generates integrated information collected around the object from wide acquisition angles into a single image. It has significant improvements in SNR, contrast and spatial resolution, artifact and speckle reduction and PSF regularization (more constant and symmetric PSF). It also has the ability to reconstruct complete edges of circular objects such as vessels and cysts which would appear as one or two semicircles on the conventional ultrasound images.

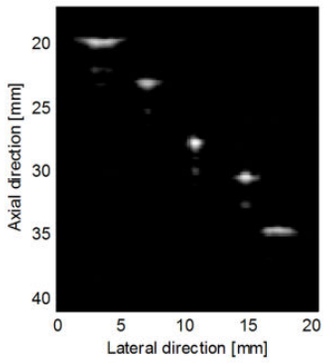

Figure 3. Variability of the PSF in the axial and lateral directions. The transducer is placed on the top of the image, and the focal distance is 27mm. The lateral resolution worsens with an increasing distance from the focal zone in either direction, superficial or deep.

2. Theory

2.1. Spatial compounding

Like in many other technological domains, researchers are still refining ultrasound imaging technology such as designing better transducers or faster systems trying to make ultrasonography more valuable. Most researches are aimed at improving on the basic paradigm of a focused scanned transducer array such as changing the geometry of element orders to make 2-D and 1.5-D arrays, increasing the numbers of the elements and reducing the sizes of the elements to improve resolution. Although the systems used today have much better resolution and cost effectiveness than prior systems, the technology is still limited by the physical behavior of sound waves. As a result, the medical application of ultrasonic imaging has seen evolutionary rather than revolutionary improvements. Combining ultrasonic imaging with spatial compounding could provide that revolutionary next-step. For instance, bones are highly reflective to sound waves. Current ultrasonic imaging techniques cannot penetrate bones, but in this research we explore large angle compounding methodologies that go around bones and other obstacles and have numerous additional benefits.

Several spatial compounding techniques, developed in the early 80's [8-10] combines multidirectional ultrasonic echoes into one image that represents the distribution of sound wave reflectivity within an area of interest. Several uncorrelated images [11] are combined in order to reduce speckle, avoid shadows, and increase contrast resolution. Combining N independent images reduces speckle contrast by an order of $\sqrt{N}$ [12, 13]. Diament et al. [14] used spatial compounding to identify stones in gall bladders and kidneys and Sehgal et al. [15] used spatial imaging to construct cross-sectional images of turkey and dog limbs. Improvements in computing, data acquisition and storage equipments, has increased the number of compounded images dramatically. The processing time is still long, however, and prevents the systems from operating in real-time in many cases. It could take two hours to do a 180-degree/110-image scan [16].

A simple example of compounding is illustrated in Figure 4. To acquire independent images without moving a transducer, the beams are electronically steered to create different incident angles. Changing the incident angle causes the obtained images to contain slightly different speckle patterns. In this case, the target of interest is a long disk-like ellipse. Placing the transducer on the top of the target Figure 4(b) results in missing information at the oblique angle. The image only contains top and bottom parts of the edges because the signal at oblique angles is reflecting away from the transducer. This phenomenon often happens when circular targets such as vessels are involved. To obtain a better contour of the target, compounding images from different incident angles such as Figure 4(a) and Figure 4(c) can help fill part of the missing edges. This type of compounding technique is usually embedded in the system without altering the ultrasound imaging techniques. Comparing the results in Figure 4(d) (with compounding) to 4(b) (without compounding), the boundaries is closer to be intact.

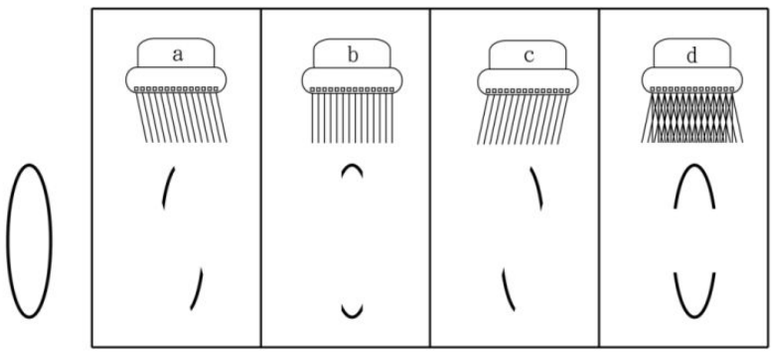

Figure 4. Illustration of conventional compounding: In panel b, the beams are generated at 90 ˚ to the surface. In panel a and c, the beams are steered to ± 12 ˚. The frames in panel a, b and c are compounded to construct a new image (frame d)

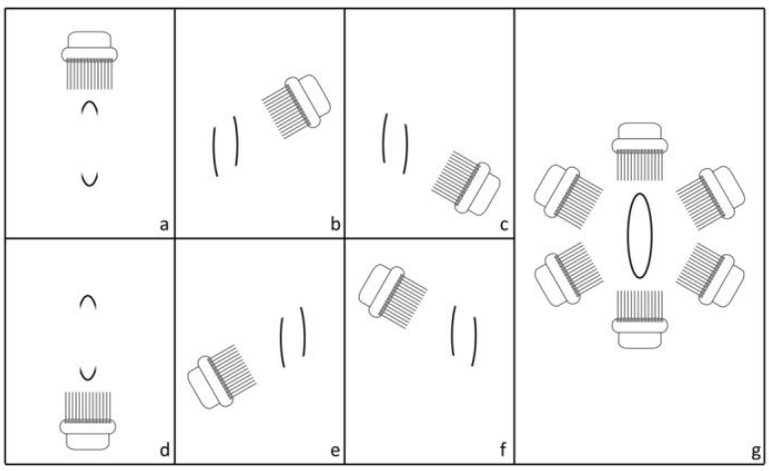

Figure 5. Illustration of supercompounding: the target is scanned from different angles on the same plane (panel a to panel f). The obtained images are compounded to construct a new image with better (complete) field of view of the target (frame g).

2.2. Supercompounding

The limitations of spatial ultrasound compounding technique stimulated research to produce an image with a complete edge (Figure 5). This concept was first used in the 80's became known as compounded ultrasound image in the 90's. In this work we investigate compounding capture angles greater than 120° and term this method as "supercompounding". In the present study, we develop a theoretical foundation for supercompounding based on our generalization of Bracewell's one-dimensional spin average concept [17, 18] to two-dimensions.

2.3. Spin average

The supercompounding technique used in this research is one kind of multi-angular spatial compounding but includes a much larger scanning range (up to 360°) than is typically employed. The target is scanned from different angles on the same plane in order to get uncorrelated data. The data contains information about the physical components as well as the artifacts. The reflected signal is variable and depends on both the incidence angle of the sound waves and the impedance mismatch within the subject. Unlike the artifacts, the primary subject of the imaging remains at the same position relative to the center of rotation while the transducer moves around the subject. Once the images are compounded together, the information of the physical components is permanent and the angular dependent artifacts are reduced.

2.3.1. One-dimensional spin average

The compounding method used in this research can be modeled using the spin average concept. One-dimensional spin average was illustrated by Bracewell [17, 18] and is given by

$$fs(r)=\frac{1}{2\pi}\int_0^{2\pi} f(r\cos\theta)d\theta \tag{3}$$

where fs(r) is the resultant function once *f(x)* is spin averaged, *r* is the radius from the center of rotation and α is the angle from axial-*x*. Assuming *f(x, y)* is a two-dimensional function which is a *rect* function in x-direction but independent in the *y*-direction. Figure 2.3 illustrates the one-dimensional spin average of a designed function stated by

$$f(x,\ y)=f(x)=rect(x/2a) \tag{4}$$

where |x| is less than *a*, *f(x)* is set up to one; otherwise, *f(x)* is zero. The value of the function indicates the height of a surface above the (x, y)-plane, and the cylindrical ridge in the y-direction shows the independence of *y*.

Instead of spinning the function, Figure 6 shows the source travelling around the center of the spinning function along the radius *r* at uniform speed to return to the starting point. The travel path is a cycle of radius *r* on *(x, y)*-plane. The spin averaged function *fs(r)* is the inte-

gral of the values passing during the course of one rotation, which gives the average heights of function *f(x)*. For this particular case, the close form solution can be derived into

$$fs(r) = 1 - (2/\pi)\cos^{-1}(a/r)H(r - a) \tag{5}$$

$$H(r - a) = \begin{cases} 0 & if r < a \\ 1 & if r > a \end{cases} \tag{6}$$

where fs*(r)* is the spin averaged function and *H* is a step function. The profile of the spin-averaged *rect* function is illustrated in Figure 7. When the translation distance is less than *a*, the travel path is on the plate form at all times. The spin-averaged values equal to one. If the translation distance is beyond *a*, the decrease of the spin-averaged value follows $fs(r) = 1 - (2/\pi)\cos^{-1}(a/r)$.

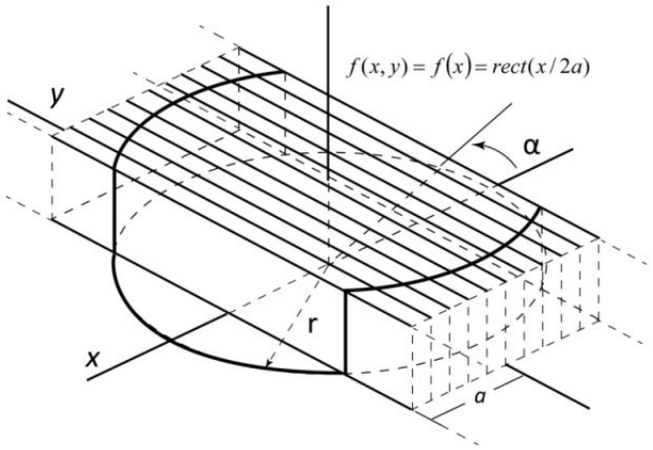

Figure 6. The illustration of equation (4): the bold curve is the travel path and its projection is a cycle of radius r on the (x, y) plane.

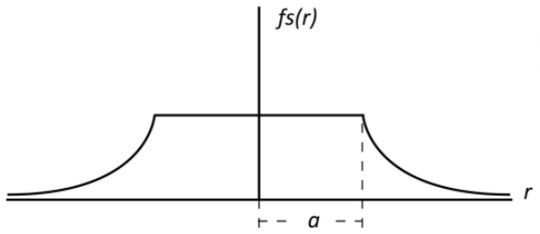

Figure 7. Profile of spin-averaged rect function: the spin averaged value starts to drop when r reaches distance a.

Alternately, we can treat the spin average as a long exposure of sound waves recorded on one image but not displayed in real time. Since sound waves are longitudinal, the beams coming from the transducer can be considered linear sources of sound, each one corre-

http://dx.doi.org/10.5772/53238

sponding to an axial line in the acquired image. When the function is being spun, the resultants are overlapped on the previous image. After one rotation, the superimposed image is the final spin average function.

2.3.2. Two-dimensional spin average

Since the y-direction is not independent in ultrasound imaging systems, we generalize Bracewell's one-dimensional spin average to two-dimension [19]. The expanded spin average function is re-written

$$f_2 s(r) = \frac{1}{2\pi}\int_0^{2\pi} f(r\cos\theta,\ r\sin\theta)d\theta \tag{7}$$

The two-dimensional spin average function is no longer independent in the y-direction; therefore, the term of *r•sinα is included in equation 7*. As comparison to one-dimensional spin average function, we have a one-dimensional rect function times a two-dimensional circ function illustrated as Figure 8 and the profile shows in Figure 9.

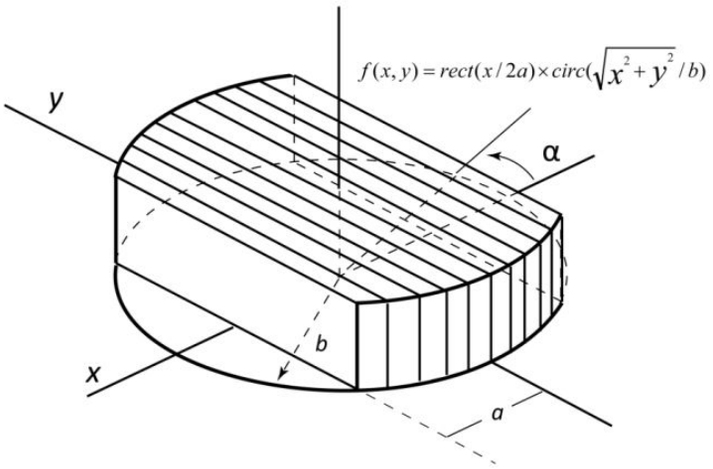

Figure 8. The illustration of equation (7): f(x,y)is a rect function in x direction and a two-dimensional circ function with radius b.

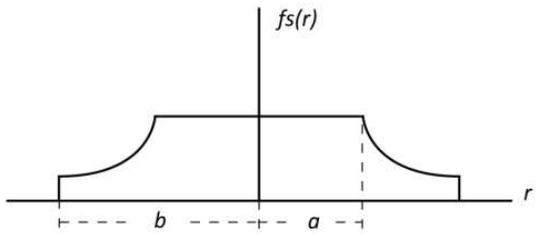

Figure 9. The profile of the two-dimensional spin averaged function

If we travel at the radial distance (r) where less than a, we are always on the top of the two-dimensional function. The value stays high. When travel at the radial distance where greater than a but less than b, the spin average value decreases and drop to zero when r equals to b.

To illustrate the concept on ultrasound image, we use numerical spin averaging on a stretched two-dimensional Gaussian function (G) which is written

$$G(x,\ y)=aexp\left[\frac{-(x\ -\ 4b)^2\ -\ (y\ -\ b)^2}{2\sigma^{\ 2}}\right] \tag{8}$$

where G represents two-dimensional Gaussian function and a is the amplitude of the function which is set to 255. σ and b are set to 4.5 and 0.2. The distribution along the x-axial is four times broader than the distribution along y-direction to simulate the PSF of a typical ultrasound system. Resolution is usually better in the axial direction than in the lateral. The stepping angle of spinning is 27.69° and it gives us thirteen images for spin-averaging. The results are shown in Figure 2.7.

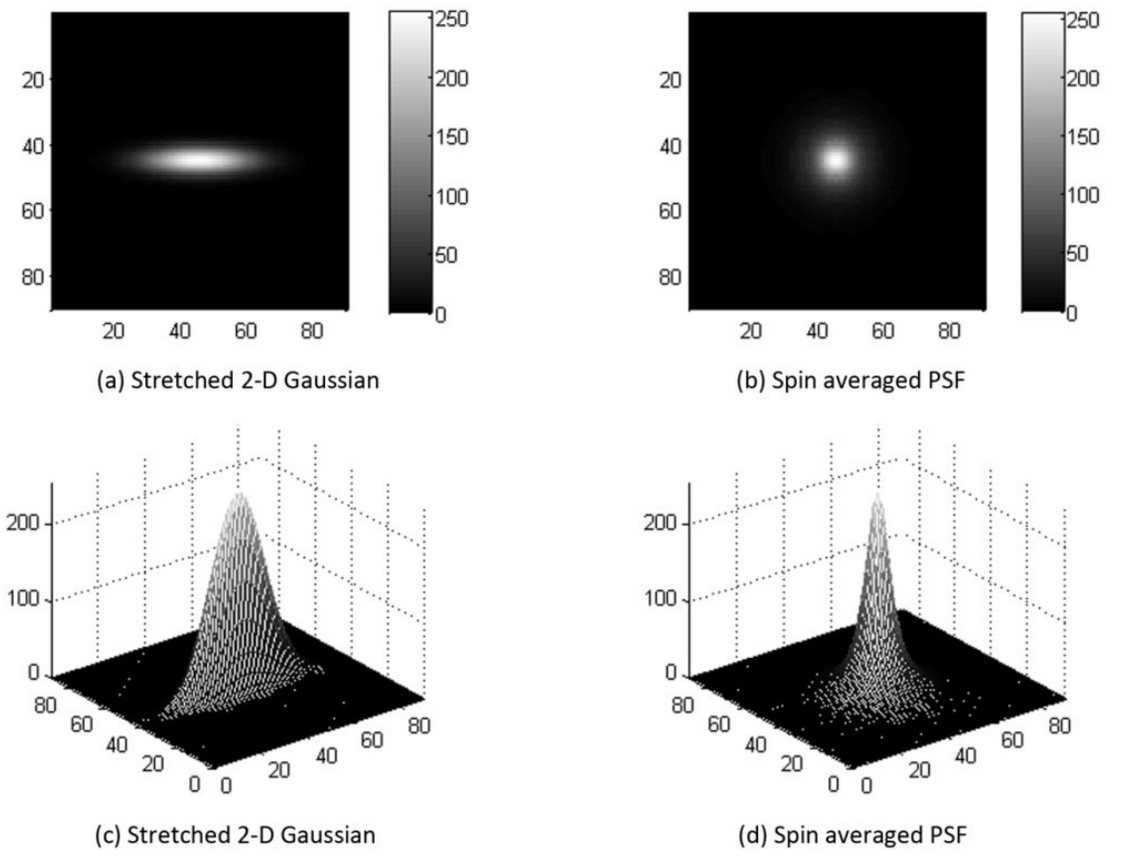

Figure 10. Spin averaging a stretched two-dimensional Gaussian function.

http://dx.doi.org/10.5772/53238

Figure 10(a) and 10(b) are two-dimensional images and 10(c) and 10(d) are three-dimensional images before and after spin-averaging respectively. Comparing 10(a) and 10(b) the image has different widths in x and y directions. After spin averaging, the resultant is more concentrate, symmetric and point-like. The profiles of the axial and lateral resolutions of 10(a) and spin averaged function of 10(b) are shown in Figure 11.

The profile of the spin average PSF (solid line) is located between the outer and inner dashed line, which represent the lateral and axial resolutions respectively. After spin-averaging, the new image becomes more isotropic. Lateral resolution is improved but axial resolution is reduced. However, the axial resolution is reduced but as return a regularized and space invariant PSF is gained. As a result, the system becomes less space-variant and the images can be further enhanced by efficient linear image techniques.

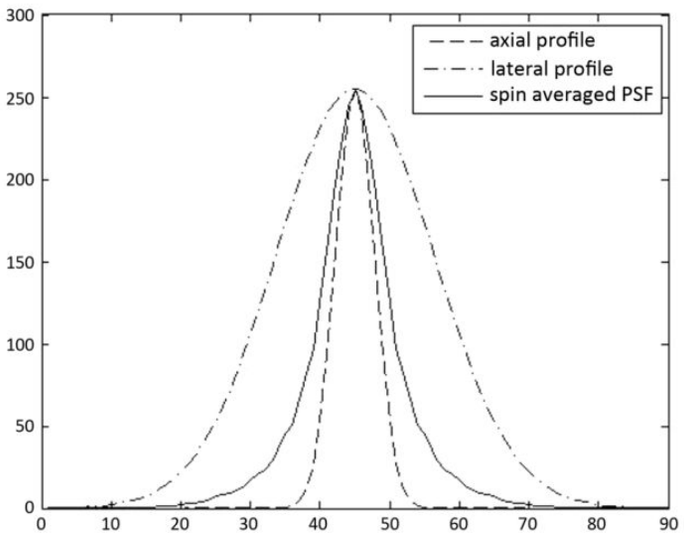

Figure 11. Profile: a. outer dashed line - lateral resolution of the stretched 2-D Gaussian function (x-direction), b. inner dashed line - axial resolution of the stretched 2-D Gaussian function (y-direction) and c. solid line - the spin averaged resolution.

In an ultrasound image, the function values (heights) while spin-averaging show the intensity of the reflected signal. In practice, these signals not only contain the information we want, but artifacts as well. Therefore, facing heights that change rapidly during the spinning will result in a high the standard deviation, which could indicate an angular dependent artifact. On the other hand, if the heights are maintained while spinning, the standard deviation is low. Thus the possibility of having a physical component located at that point is high. Therefore, spin average keeps a fairly high amount of intensity values of the physical components, and reduces the intensity of artifacts. Hence, the contrast resolution is enhanced.

2.4. Regularized point spread function

Spin average reduces artifacts, reveals the true shapes of physical components and regularizes the point spread functions which means having a more symmetric, more uniform and tighter PSF which is less space invariant. For practical purposes, the quality of results is inversely related to the size of the travel step α. The regularization of the PSF function is shown in Figure 12. In this illustration, a metal pin head is used to simulate a point target.

In Figure 12(a) the PSF resultant picture shows an upside down triangle with long wings. Since the physical shape of the target is a point, the level of artifacts will be high. The axial reverberation is angular dependent artifacts, and the size of lateral resolution is limited by both the transducer and different focal zones. By reducing the stepping angle of spinning α from 0° (360°) to 60°, and then to 30°, the compounded PSF shrinks to a point (Figure 12(b), (c)). This suggests that the spin average can remove the angular dependent artifacts and distortion caused by focusing.

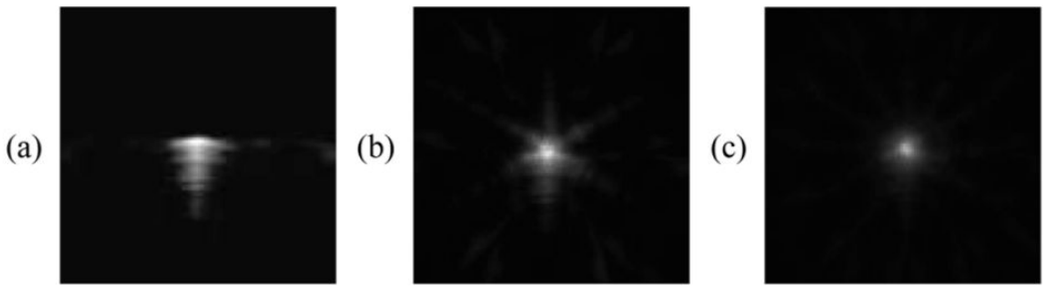

Figure 12. The PSF of a metal pin head (a) the original PSF without spin average - α = 0° (b) the PSF with 6 images compounded - α = 60° (c) the PSF with 12 images compounded - α = 30°

3. Materials and methods

3.1. Introduction

The experiment setup focuses on utilizing a conventional ultrasound imaging system (GE RT-3200) to test the spin average theory and the supercompounding concept. The experimental apparatus – the three-dimensional moving platform – is designed in two parts, image acquisition and image processing.

Since a complete spin average is an integral between 0 and 2π, the images or data has to be acquired around the targets of interest. In order to do so, either a transducer has to be rotated around the targets or the targets themselves have to be rotated around the center point. The latter option – objects rotating around a center point – is used in this experiment to achieve better results in demonstrating the concept of the spin average theory and supercompounding technique. One reason to favor this option is that the rotation of the targets of interest allows us to accomplish the goal without moving or vibrating the transducer. Another reason is that the transducer will always have solid contact with the surface of the tar-

http://dx.doi.org/10.5772/53238

get container. As a result, our objects are mounted on a rod connected to a DC gear motor controlled by a micro-controller.

The same micro-controller also controls image acquisition. Once the target is rotated to the designed angle, the micro-controller triggers the frame grabber to capture the image and to store the results in a specific order. Such order is the index for quantifying the rotational degree of the images.

Since the conventional ultrasound images are usually shown in the vertical axial direction, the transducer is positioned at the top of the image shown as Figure 13. In order to have all images aligned in the same coordinate system, a coordinate transformation (derotation) has to be applied on each image at a specific angle based on the rotation index around the center of the rotation. After derotation, all images are ready for the recombination, which completes the supercompounding process.

3.2. Work flow

The work flow of the experiment is as illustrated in Figure 14(a). The target is submerged in a water tank illustrated as Figure 14(b), muffled with foam material on the rear, lateral, and bottom sides to reduce the surplus reflection of sound waves. The sound wave form is generated and detected by the ultrasound transducer and the results are sent to the ultrasound console (GE RT-3200) for detection and processing to form real time ultrasound images. These images are simultaneously shown on the screen of the RT-3200 and the display of the frame grabber. Once the micro-controller drives the subject to the designed angle, it triggers the frame grabber to capture and store a still image, which then moves on to the next designed angle; the process repeats until the micro-controller completes a 360 degree scanning. These still images are stored in sequence as the rotation index. The whole set of images is used to construct one final supercompounded ultrasonography.

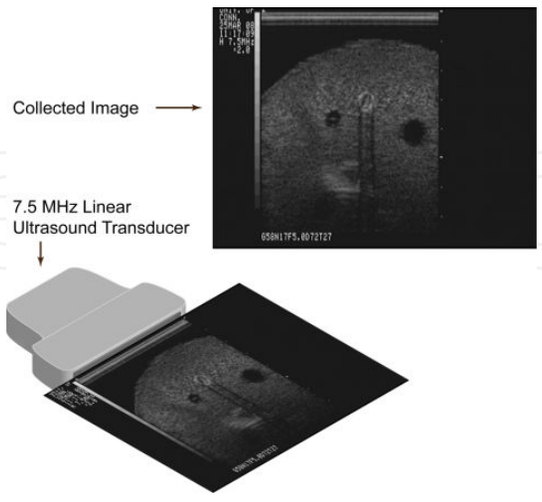

Figure 13. Illustration of the relative positions between the collected image and the ultrasound transducer. The image shows the vertical axial direction with the image plane perpendicular to the surface of the ultrasound array. The specific 7.5 MHz linear ultrasound array shown above has 128 elements. With two times of zoom-in setting, it covers two-thirds field of view.

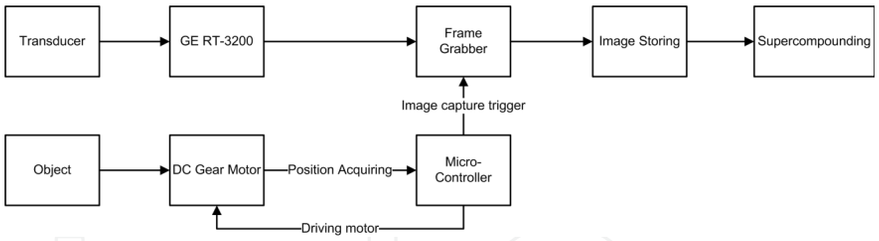

(a) Work flow

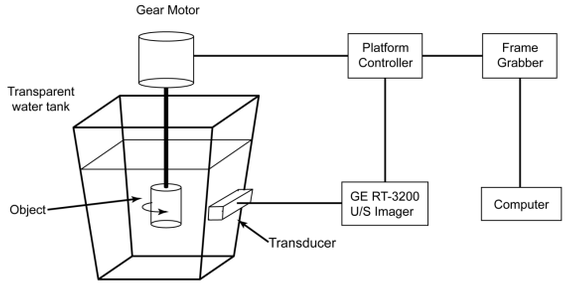

(b) Illustration of the experiment setup

Figure 14. The work flow and the illustration of the experiments setup. The target of interest is mounted on the output shaft of the DC gear motor. Micro-controller controls the rotation of the motor. Once it is rotated to the designed angle, the micro-controller sends capturing signal to the frame grabber to store the image that is concurrently being received from the GE RT-3200 ultrasound console.

3.3. Processing of ultrasound images

3.3.1. Software

The software used to process the raw image data for supercompounding is MATLAB (matrix laboratory). MATLAB is a numerical computing environment that allows matrix manipulations, plotting functions and data and implementation of algorithms to solve the mathematic issues. Behind the mathematic operations, it is also a tool to create a user interface, correlating with programs written in other languages, such as C++.

The reasons why MATLAB is used to process the resultant images are (1) the image itself is a matrix and (2) manipulating matrices is one of the major strengths of MATLAB. With many built-in tool boxes, most of the ordinary image operation can be accomplished easily.

3.3.2. Images

The image is pixelized data. Each pixel (point) in the image corresponds to an intensity value ranging from 0 to 255, the dynamic range of the display. In an ultrasound imaging system, the image is black and white, or in the so-called "gray scale". "Zero" represents black and "255" represents white. Between black and white there are different shades of gray illustrated as Figure 15.

Figure 15. Illustration of the dynamic range of a gray scale image. Values between absolute black and white are divided into 255 levels. These levels are called "gray levels".

The resulting images are stored as bitmap image files (bmp) in a 24-bit bitmaps format including three color layers (green, blue and red). Bitmap data (pixel array) describes the image pixel by pixel. 24-bit represents 24 bits per pixel. For instance, the recorded ultrasound image in the experiment is 640 pixels by 480 pixels. That leads to 307,200 pixels in total. Each pixel is 24 bits, which gives us 7,372,800 bits per image, 921,600 bytes (1 byte = 8 bits) or 900 k (1 k = 1024 bytes) in other words.

Since the ultrasound images used in the experiment are black and white (gray scale) images, the data recorded in the three color layers are the same. To reduce image processing time, only one layer of data is used. The layers are segregated and only the green layer is kept. It leads to a smaller image size – 300k (one-third of 900k).

3.3.3. Image rotation

As is stated in the discussion in section 3.1, to process the spin average concept, involved images must be in the same coordinate system. Each individual image has to be derotated around the center of rotation (corresponding to the relative position between the ultrasound transducer and the output shaft of the gear motor shown as Figure 16).

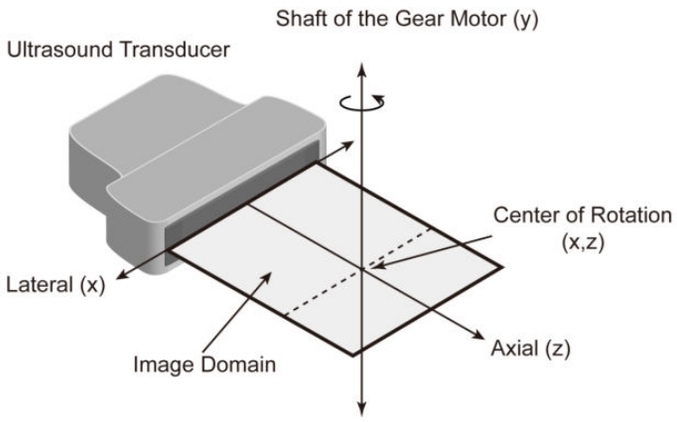

Figure 16. Illustration of the relative position between the shaft of the gear motor and the ultrasound transducer. In the experiment, the object is mounted on the output shaft of the gear motor and is rotated at the center of rotation.

Figure 17 (a) and (b) illustrate how a triangular object is imaged. (a) is taken when the object is at the starting position. In order to perform spin average concept, the object has to be imaged from other angles. (b) is collected when the object is rotated 30 degrees counter clockwise around the center of the rotation. (c) and (d) are the results of (a) and (b) respectively. As the results shown in (c) and (d), the objects are shown in two different coordinate sys-

tems. Therefore, a coordinate transformation has to be performed on the images to keep the objects in the same coordinate system. A 30-degree-clockwise rotation is performed on Figure 17 (d) to transform the image to the same coordinate system as (e) which is 0 degree rotation from (c). Since the coordinate transformation is the second time of rotation and is in the opposite direction to neutralize the first time of rotation, we call it derotation.

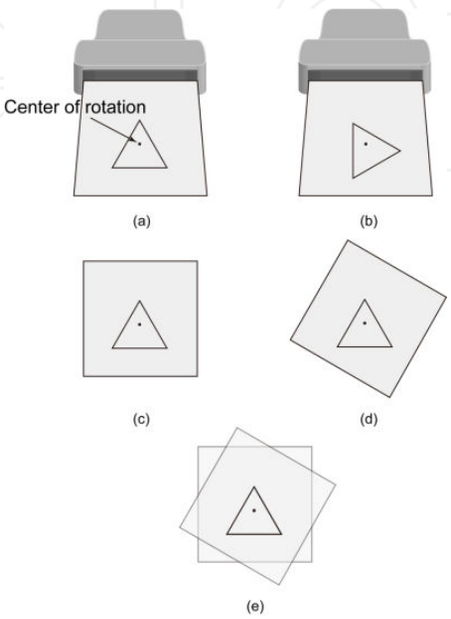

Figure 17. Illustration of derotation. (a) and (b) illustrate how a triangular object is rotated and then imaged. (c) and (d) are the images after derotation. (e) is the compounded image of (e) and (f).

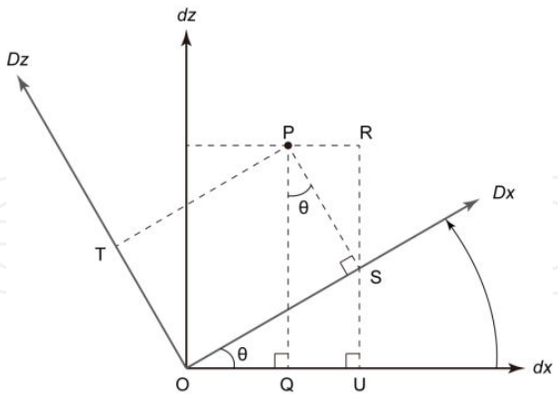

Figure 18. dx and dz are the initial axes and Dx and Dz are the rotated axes by θ. P is the demonstration point and O is the origin.

All images are electronically derotated around the center of rotation in MATLAB. Coordinates mapping the derotated images to the initial position can be obtained using the standard formula for axes rotation [20]:

$$\begin{cases} Dx = dx\cos\theta + dz\sin\theta \\ Dz = dz\cos\theta - dx\sin\theta \end{cases} \tag{9}$$

where dx and dz are distances of the pixel from the center of rotation, Dx and Dz the new coordinates after transposition. The relationship between initial and rotated axes (shown as Figure 18) can be derived geometrically.

The coordinates of P on dx-dz plane is $(\overline{OQ}, \overline{QP})$ and is $(\overline{OS}, \overline{PS})$ on Dx-Dz plane.

$$\begin{cases} \overline{OQ} = \overline{OU} - \overline{QU} = \overline{OS}\cos\theta - \overline{PS}\sin\theta \\ \overline{PQ} = \overline{RS} + \overline{SU} = \overline{PS}\cos\theta + \overline{OS}\sin\theta \end{cases} \tag{10}$$

The relation in general form is denoted as following equations.

$$\begin{cases} dx = Dx\cos\theta - Dz\sin\theta \\ dz = Dz\cos\theta + Dx\sin\theta \end{cases} \tag{11}$$

Equation 11 can be solved and rewritten as equation 9.

3.3.4. Supercompounding

As discussed in section 2.3 and 2.4, the supercompounding technique is based on the two-dimensional spin average concept. To satisfy equation 7 in practice, the discrete method is used in the present study. By rotating the object and summing a multiplicity of images, we can approximate a continuous spin average. In theory, the rotational stepping degree θ is infinitely small. In practice, the angular stepping degree of the motor represents the travel step in the theory and equation 7 can be rewritten discretely as the following equation,

$$f_2s(r) = \int_0^{2\pi} f_d(r\cos\theta, r\sin\theta)d\theta \tag{12}$$

$$f_2s\left(r\right) = \frac{1}{N}\sum_{M=1}^{N} f_d(r\cos M\theta, r\sin M\theta) \tag{13}$$

where $f_2s(r)$ is the two-dimensional spin average function, f_d represents the image domains after the derotation process, θ is the stepping degree, M is 1,2,3,…,N and N is the total number of the derotated images ($N=2\pi/\theta$). Either equation 7 or 12 is described in the polar coordinate system. To process the concept on the images which is described as a pixel grid, Cartesian coordinate system can be used to further simplify the process illustrated in the following equation,

$$f_2 s\left(Dx,\ Dz\right) = \frac{1}{N}\sum_{M=1}^{N} f_{d,M}(Dx,\ Dz) \tag{14}$$

where Dx and Dz are coordinates in Cartesian system after the derotation transformation and $f_{d,M}$ represents the numbers of derotated images. Once the raw images are derotated properly, they can be substituted into equation 13 easily. The process can be broken down into three phases, (1) derotate raw images, (2) superimpose derotated images and (3) average the result. The illustration and the example of the supercompounding process are shown as Figures 19 and 20.

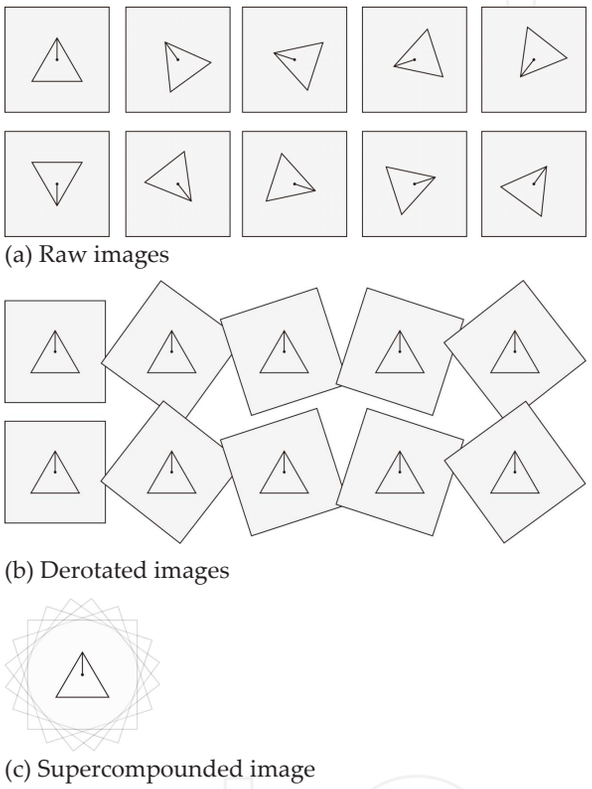

(a) Raw images

(b) Derotated images

(c) Supercompounded image

Figure 19. Illustration of the supercompounding process. The triangular object is rotated every 36 degrees counterclockwise and it makes the clockwise derotation. The supercompounded image is the superimposed image of all derotated images.

4. Results

In this research, two objects are studied: the metal pin heads and the dissected porcine aortic root. Each object is chosen for different purposes and together allows us to observe the performances of the spin average concept and the supercompounding technique under different circumstances. These selected objects also represent some issues that conventional ultrasound imagers face, which include the following:

- Non-circular point spread function (PSF): As stated in section 2.4, the PSF is not a circular point in the conventional ultrasound imagers. This is because the lateral resolution is several times worse than the axial resolution. Therefore, after the image convolves with the PSF, the output image from the ultrasound system could be several times more blurred in the lateral direction than in axial. To evaluate the supercompounded PSF, the metal pin head is selected.
- Circular object: Circular objects generally do not appear circular on ultrasound images. The edges of the two-side walls are usually missing because the incident ultrasound waves are reflected away-from instead of back-to the transducer. The ultrasound system cannot receive any signals coming from those regions and causes the image to dropout at oblique angles. The dissected porcine aortic root is used to test the imaging performance of circular objects like blood vessels or cysts. The tests of the aortic roots are collaborated experiments with Dr. Wei Sun [21] (Biomedical Engineering, University of Connecticut).

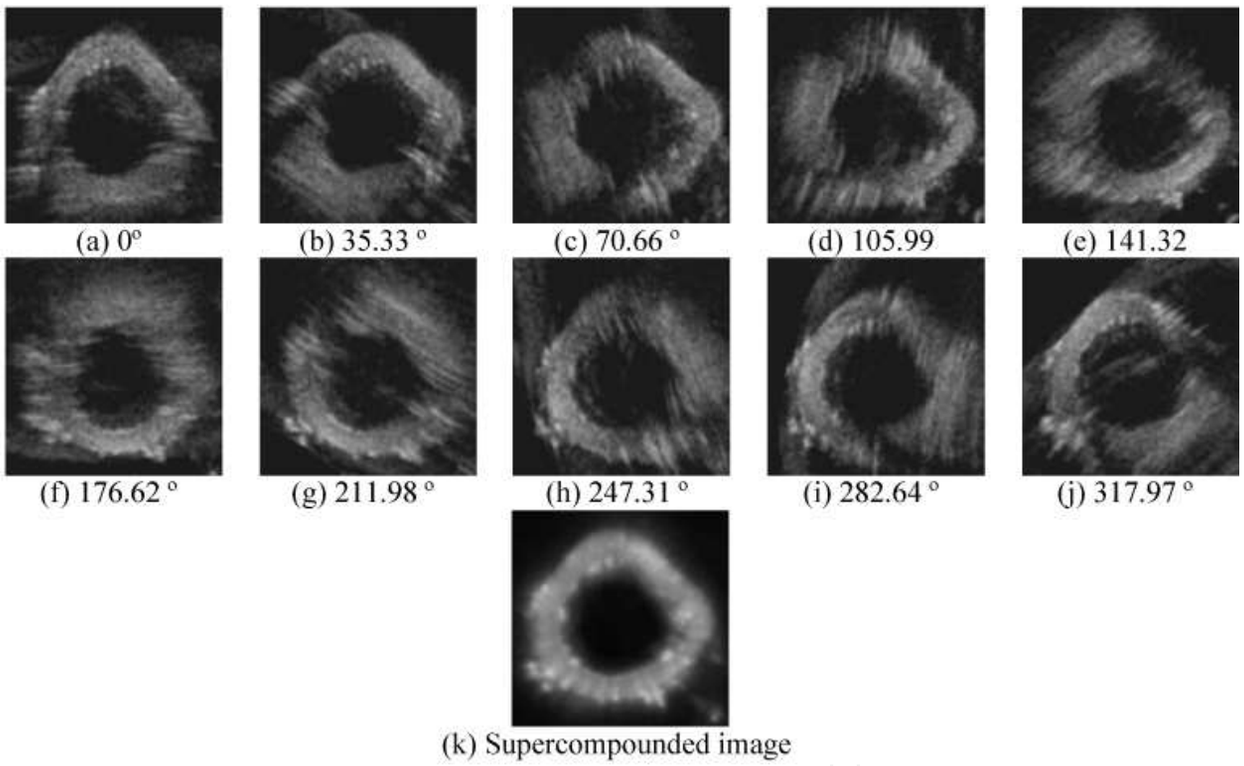

Figure 20. Example of supercompounding process with a porcine aorta. The results of (a) to (j) are the part of the derotated images taken from the every 1.68 degrees. (k) is the supercompounded image superimposed from 214 derotated images. Note multiple nodes of enhanced echogenicity become clear after supercompounding.

4.1. Imaging of metal pin heads

The metal pin heads used in the study are 0.5 millimeter diameter pin heads. They were selected for their small size and for their material, which is highly reflective when placed in water due to the acoustic impedance mismatch. Sound waves that hits this material cause

massive reverberation, i.e. multiple reflections, in which create parallel lines under the object on the ultrasound images. Therefore, in addition to observing the offset of improving the point spread function, this test can be used to observe how supercompounding handles reflective material layers. Figure 21 is one of the raw images of the metal pin heads. The metal pin heads are arranged as a capital letter 'L'. All images are taken with the 7.5MHz linear transducer.

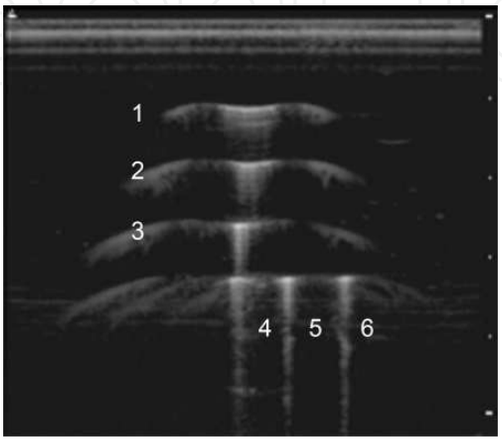

Figure 21. Metal pin heads are arranged as a letter L. The six objects are shown as "T" like shape instead of point like. The axial artifacts are caused by the reverberations inside the metal pin heads. The reverberations mislead the ultrasound imager that there are the same objects in consecutive depths. It makes multiple lines behind the objects. The pin number 1 to 3 and group 4, 5 and 6 are aligned at different depths. The focal zone is 27 millimeter in depth. It is at the middle of the pin number 3 and group 4, 5 and 6; therefore, the pin number 1, 2 and 3 are superficial to the focal point and the group 4, 5 and 6 are deep to the focal point.

Figure 21 shows artifacts on the image of six objects caused by reverberation. The objects are the metal pin heads and they should appear point like instead of a T-shaped with long tails (reverberations) and wings (side lobes). As stated in section 2.4, the point spread function is space variant in most conventional ultrasound imagers and causes size differences for the same objects depending on how far the object is away from the focal zone. In Figure 21, each pin represents the point spread function at one spatial position. The measurements of dimensions are described in Table 1.

Pin number	Lateral size	Axial Size	Depth
1	46 px	3 px	11.30 mm
2	31 px	4 px	17.99 mm
3	11 px	3 px	25.32 mm
4	13 px	4 px	31.80 mm
5	13 px	3 px	31.80 mm
6	13 px	3 px	31.65 mm

Table 1.

http://dx.doi.org/10.5772/53238

Pins 1-6 are all either three or four pixels in axial size regardless on reverberation artifacts. This translates to an average size of 0.56 ± 0.086 mm.

The lateral sizes, however, vary depending upon the depths and the distance from the focal zone. The pin closer to the focal zone (27 mm) has better lateral resolution. The average size in the lateral direction is 3.59 ± 2.38 mm, which is seven times larger than the actual size. The best result is the pin number 3. It is 1.7 mm away from the focal zone (27mm – 25.32mm = 1.7mm), and with a lateral size is 1.83 mm, it is still three times larger than the actual size of the metal pin head. Figure 22 compares the raw image with the supercompounded image constructed from 214 derotated raw images.

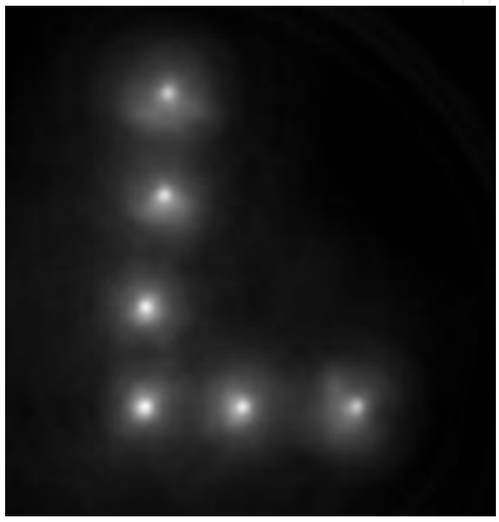

Figure 22. Supercompounded image. Comparing to Figure 4.1, the artifacts are significantly reduced and the result shows each point has similar circular shape and is tighter and more symmetric.

In Figure 22, six points appear instead of the T-shape. The artifacts from reverberation are significantly reduced as well. The measurements are included in Table 2.

Pin number	Lateral size	Axial Size	Depth
1	5 px	6 px	N/A
2	5 px	5 px	N/A
3	5 px	5 px	N/A
4	4 px	6 px	N/A
5	4 px	4 px	N/A
6	4 px	4 px	N/A

Table 2.

The average size in lateral direction is 0.86 ± 0.09 mm and 0.835 ± 0.15 mm in the axial. They are one and half times larger than the actual size of the pin head in all directions. As discussed in section 2.5, the supercompounded PSF should be closer to the axial resolution.

4.2. Imaging of dissected porcine aortic root

The study objects in this section are dissected porcine aortic roots. Each target is scanned under different pressures and levels (Figure 23), and the images are taken during the inflation test of the aortic root. The inflation test simulates the mechanical response of the aorta under different blood pressure ex-vivo. Different stress levels are simulated when the hydrostatic pressure supply inflates the target.

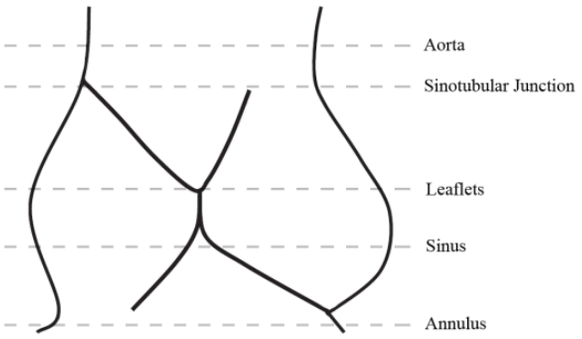

Figure 23. Illustration of aortic root. The root is scanned at five different levels named aorta, sinotubular junction, leaflets, sinus and annulus.

The study is focused on the geometry of the aortic valve, which can be used as a standard model to calculate volume changes during the inflation test. The raw images are collect with the 7.5MHz linear transducer. In this research, after derotating and spin averaging the 214 pictures, the resulting supercompounded picture at aorta level is shown in Figure 24 and Figure 25.

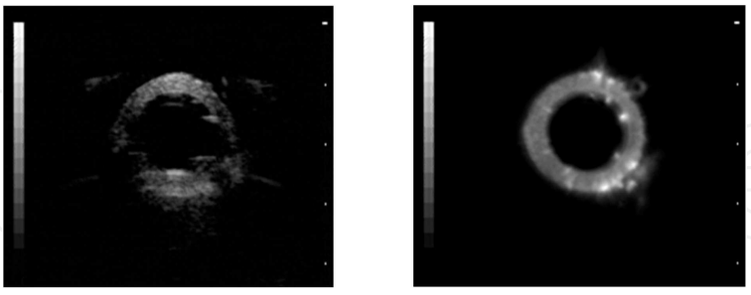

(a) raw image (b) Supercompounded image

Figure 24. The dissected porcine aortic root at aorta level.

The raw B-scan image Figure 24(a) shows sound waves that are dropped-out (region 2 and 3 in Figure 25) at the oblique angles to the normal line of the tissue structure interface. This phenomenon happens when circular shape objects (such as vessels) or spherical objects (such as cysts) are imaged. The supercompounded image (Figure 24(b)), constructed by multi-angular images with an independent viewpoint, exposes each segment of boundary to

http://dx.doi.org/10.5772/53238

normal incidence, thus reducing dropout. The entire vessel is symmetrical and intact and spots like echogenicities (arrows in Figure 25) become visible in the supercompounded image. The supercompounding technique enables the observation and study of these echogenicities and their properties.

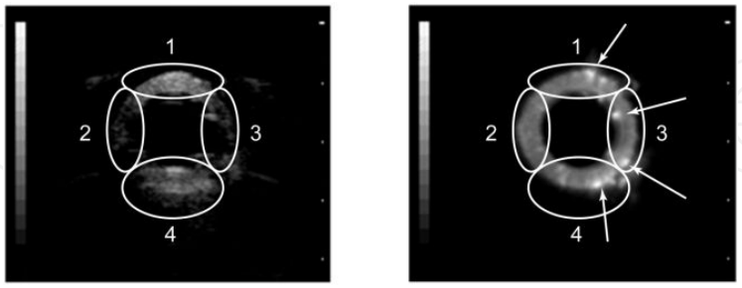

(a) raw image (b) Supercompounded image

Figure 25. Comparison results of the dissected porcine aortic root at aorta level. Region 1 is the superficial area. It is close to the focal zone. It makes the best part of result on the raw image. Region 2 and 3 are the dropout areas. Because of the shape of structures in the regions are at the oblique angles to the incident ultrasound waves, the ultrasound waves are not reflected back to the transducer. It makes missing edges on the image. Region 4 is the out of focal zone area. Due to the worse PSF and the attenuation of the ultrasound waves, the structures in the area are not described accurately comparing to the same region on the supercompounded image. In the region 4 of the supercompounded image, the structures are clear and sharp, but they are blurry and several times larger on the raw image. The arrows point out the echogenicities which are not appeared on the raw image.

Not only can supercompounding fill the portions of tissues missed by conventional ultrasound imagers, but also can markedly reduce speckle noise in the image. The results shown in Figure 26 and Figure 27 are the aortic roots at leaflets level. Professionally trained eyes might be able to distinguish between an aortic root and the leaflet. Untrained eyes will find it hard to determine the boundaries and the size of the root.

In the raw image Figure 26 (a), the boundary is not clear especially away from the focal zone (region 5 in Figure 27) where is deep to the focal zone of the image. The supercompounded image Figure 26 (b) shows clear edges and details. We can now easily determine the location of the leaflets (region 2, 3 and 4 in Figure 27). The supercompounded image offers a better field of view as well, making the image more valuable and easier to read.

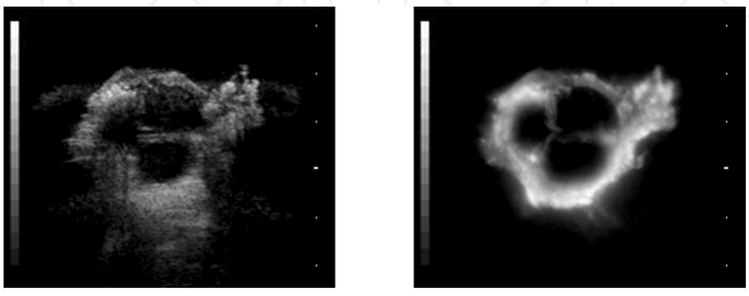

(a) raw image (b) Supercompounded image

Figure 26. The dissected porcine aortic root at leaflets level.

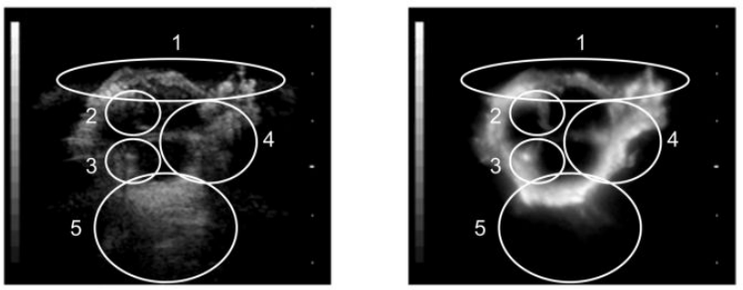

Figure 27. Comparison results of the dissected porcine aortic root at leaflets level. Region 1 is the area having the best result which is close to the focal zone. Region 2, 3 and 4 are the areas show three leaflets. As the result on the supercompounded image, three leaflets appear clearly. However, on the raw image, only the region 4 indicates or suggests a leaflet. The other two in the region 2 and 3 are barely recognized as leaflets. Region 5 is the deep area. It is out of the focal zone. Affected by the worse PSF and the attenuation of the ultrasound waves, the structures are not even close to the real object in the region.

5. Discussions and conclusions

Supercompounding is an innovative and still developing space compounding technique. It can be applied to traditional ultrasound imaging systems. As shown as this research, the supercompounding technique can provide dramatic improvement to the quality of ultrasonography of typical biologic tissues. The speckle, artifacts and reverberation are reduced, and we are able to visualize complete edges especially at oblique angles to the front of beam direction. However, these are not the only benefits of supercompounding. By utilizing the two-dimensional spin average theory it was shown that supercompounding can improve spatial resolution by regularizing the point spread function. It is a critical improvement to have an ultrasound image with a regular or space invariant point spread function that can potentially enhance performance by application of linear systems of signal processing algorithms.

Validation of supercompounding includes two main activities: ultrasound image acquisition and supercompounding processing. Ultrasound image acquisition includes the design and the construction of a three-dimensional moving platform. The platform allows the imaged object to rotate 360 degrees for testing the spin average concept and also to move in three directions for constructing a three-dimensional voxel set of information of the object, a set that could be used to produce a three-dimensional image.

The supercompounding processing has evolved in two sub branches: preprocessing and post-processing algorithms.

- Preprocessing technique produces a supercompounded image from derotating and combining the acquired raw image set. It is considered a preprocessing because the proposed supercompound imaging overcomes some of the physical limitations of ultrasound signals. It reduces speckles, shadows and reverberations and gives a regularized point

spread function across the ultrasound images. For example, a shadowed region in conventional ultrasound cannot be restored since the data is simply not present, or the point spread function may obscure fine details beyond the ability of post-processing to retrieve it. Another aspect to consider is that post-processing may be based on preconceived notions of what certain image regions should look like, thus providing inaccurate information of the imaged anatomy. Consequently, we consider the use of preprocessing techniques to be preferable as they provide "true" improvements in SNR and resolution [22].

- A regularized point spread function makes post-processing algorithms [22] (image enhancements) more beneficial to the supercompounded image, especially for linear systems algorithms like image deconvolution. By utilizing the two-dimensional spin average theory, supercompounding is shown to improve spatial resolution by having a regularized and tighter point spread function. Due to space variant resolutions in both axial and lateral directions, the point spread function of ultrasound image changes. Therefore, it is essential to have an ultrasound image with a regularized point spread function for further application of many signal processing algorithms. There is less need to make an assumption of the space invariant point spread function or to discretize the processed image into small pieces working windows when we process the ultrasound images.

- For example, a regularized point spread function can simplify the frequency filtering or deconvolution process which is one of the most straight forward and effective image sharpening methods. As discussed in section 2.1, the obtained image can be modeled as the result of a raw image convolving with a point spread function. This convolution is a blurring process. In order to get back to the original sharp image, the reverse process, namely "deconvolution", is required to restore the image before it convolves with the point spread function. However, it is not directly applicable on ultrasound images because of the space variant point spread function. Therefore, the deconvolution is applied regionally or not at all. Since the supercompounded image has a symmetric and regularized point spread function, the deconvolution process can be applied to the whole image without segmenting it [4, 23, 24]. Thus supercompounding provides a higher quality preprocessed image and also makes post-processing applications more viable and effective.

5.1. Supercompounding applications

The results in this study suggest that the spin average concept and the supercompounding technique can dramatically improve the quality of the ultrasound images. The following list points out three ways to utilize the supercompounding technique in clinically:

- Extremities: The supercompounding applicant could be utilized on extremities. It is easy to gain 360 degrees access around the extremities and usually the ultrasound waves can at least penetrate half of the thickness of the extremities (from superficial skins to the bones in the middle) even with higher frequency ultrasound transducers. It could potentially be a great way to diagnose and evaluate abnormalities of the muscles and the tendons, especially for sport medicine.

- Neck: The supercompounding technique could also be used on the neck for diagnosis of carotid atherosclerosis. If plaque builds up in the body's arteries, the condition is called atherosclerosis. Once the built up plaques narrow the common carotid arteries, the patient is under a high risk of cerebral flow reduction or stroke because of the reduced blood flow. The diagnosis is often evaluated by CT or multidetector-row CT angiography (CTA) [25] which utilizing ionizing radiation. Supercompounding ultrasound could offer a safer way to make the same diagnosis. The plaque is often calcified which particularly late stage can make it highly reflective. It can show high intensity on the ultrasound image. Plaques can be identified relatively easily. With the help of the supercompounding technique, the disease could be diagnosed more cost-effective and without exposing patients to the ionizing radiations once a proper mechanical supporting apparatus is designed for 360 degrees scan around the neck.
- Abdomen: Ultrasound imaging is widely used to image certain organs in the abdomen such as the liver, kidneys and pancreas. However, the evaluation is highly related to experiences and training of the radiologist. For instance, a patient who has liver cancer could have different kind of reports depending on the image reading whether by radiologists or other professionals. Imaging can provide information on extend of metastasis often diagnosis of cancer is made. Abdominal ultrasound imaging usually is performed with low frequency transducer and has low resolution results. It is radiologists' responsibilities to discover the abnormalities. With the help of supercompounding, it could reduce the odds for such error. It would be easier for radiologists to identify abnormalities. Abdominal imaging is made challenging due to the thickness of the belly and the bowels (small and large intestines) which are filled with gas which blocks ultrasound propagations. Therefore, ultrasound in the abdomen is limited to a few "windows" where the probe can bypass the intestines and gain access. Even with the 3.5 MHz transducer (which is close to the lowest frequency presently used for ultrasound imaging), it is hard for the ultrasound waves to penetrate through the whole abdomen. There are two possible solutions to the task: one is to perform partial supercompounding and the other is to further lower the ultrasound frequency. The partial supercompounding might not help construct an image with complete edges of the object, but it could still be much better than one single raw image according to the spin average concept.

The second solution is to image the abdomen with lower ultrasound frequency such as 1-2MHz. The ultrasound waves might be able to penetrate through; however, the resolution might be worse than using 3.5MHz transducer since for such low frequency, the corresponding wavelength of sound (at 1MHz) is 154mm, assuming the speed of sound is 1540 m/s in soft tissue. It means the two objects have to be at least 154mm away from each other to be identified as different objects on the ultrasound image when 1MHz transducer is used. Comparing two supercompounded images constructed from raw images scanned by the 7.5MHz and the 3.5 MHz transducers, there is no significant resolution reduction between the two supercompounded images, which is highly noticeable when we compare the two

raw images from the two transducers. This suggests that the resolution of the supercompounded images is not affected as much as the traditional raw images when we lower the frequencies of the ultrasound transducers. It is potentially a good way of obtaining a satisfactory resolution of the supercompounded image with lower frequency transducer without sacrifice of ultrasound penetration.

5.2. Conclusions

Advances in the technology of transducers, semiconductor devices, and computers have supported the implementation of enhancement techniques and the development of the industry of ultrasound in general. The present ultrasound imagers can provide higher signal-to-noise ratio and utilize transducer arrays with increasing numbers of elements. Consequently, the quality of the images has improved significantly especially compared to the earlier generation ultrasound imager used in the study (GE RT-3200). However, there has been no major breakthrough from physics point of view. The limitations of ultrasound imaging still remain such as the trade-off between penetration and frequency (resolution), space variant point spread function and sound wave self interference (speckle). These limitations sometime have become part of the ultrasound imaging, and by well training, radiologists or sonographers can work around them to some degree.

If it is possible to obtain higher quality tomographic images of the human body with ultrasound, the use of this technology can be extended to other applications where currently CT and MRI are used and make diagnosis more accurate, safer and more cost-effective for radiologists or sonographers. The proposed supercompounding imaging of ultrasound is a good approach to make ultrasound imagers perform beyond their present limitations. It works in harmony with the technology of modern ultrasound imagers. Supercompounding will benefit from better ultrasound transducers. The advantages would be to avoid the exposure of the patients to ionizing radiation and the availability of high quality soft tissue medical imaging at reduced cost. The unique sensitivity of ultrasound to soft tissues also makes it qualitatively superior to X-rays for many applications and it is a much faster modality than magnetic resonance. Overall we feel this technology could provide the impetus for an entire new generation of ultrasound imaging.

Author details

Tsuicheng D. Chiu[1], Sonia Contreras[2] and Martin Fox[3]

1 Biomedical Engineering, University of Connecticut, Storrs, CT, USA

2 Electrical and Electronic Engineering Program, Universidad Tecnologica de Bolivar, Bolivar, Colombia

3 Electrical & Computer Engineering, University of Connecticut, Storrs, CT, USA

References

[1] R. H. Gottliev, "Imaging for Whom: Patient of Physician?," American Jorunal of Roentgenology, vol. 185, pp. 1399-1403, 2005.

[2] J. J. Cronan, "Ultrasound: Is There a Future in Diagnostic Imaging?," Journal of the American College of Radiology, vol. 3, pp. 645-646, 2006.

[3] J. F. Moreau, "Re: "Ultrasound: Is There a Furture in Diagnostic Imaging?"," Journal of the American College of Radiology, vol. 4, pp. 345-357, 2007.

[4] T. Chiu, et al., "Supercompound imaging with Weiner deconvolution," in Proc. SPIE 7265, Orlando, FL, 2009.

[5] I. P. Herman, Physics of the Human Body. New York: Springer, 2006.

[6] R. F. Wagner, Smith,S.W.,Sandrik,J.M. and Lopez,H., "Statistics of Speckles in Ultrasound B-Scans," IEEE Trans. on Sonics and Ultrasonics, vol. 30, pp. 156-163, 1983.

[7] A. K. Jain, Fundamentals of Digital Image Processing. Englewood Cliffs, NJ: Prentice Hall, 1989.

[8] G. Wade, "Ultrasonic Imaging by Reconstructive Tomography," Acoustical imag., vol. 9, pp. 379-431, 1980.

[9] J. Greenleaf and R. Bahn, "Clinical Imaging with Transmissive Ultrasounic Computerized Tomography," IEEE Trans. Biomed Eng, vol. 28, pp. 177-185, 1981.

[10] D. E. Robinson and P. C. Knight, "Computer reconstruction techniques in compound scan pulse-echo imaging," Ultrasonic Imaging, vol. 3, pp. 217-234, 1981.

[11] C. B. Burckhardt, "Speckle in Ultrasound B Scans," IEEE Trans. Sonics Ultrason., vol. SU-25, pp. 1-6, 1976.

[12] P. M. Shankar, "Speckle Reduction in Ultrasound B-Scans Using Weighted Averaging in Spatial Compounding," Ultrasonics, Ferroelectrics and Frequency Control, IEEE Transactions on, vol. 33, pp. 754-758, 1986.

[13] Trahey, et al., "Speckle pattern correlation with lateral aperture translation: experimental results and implications for spatial compounding," IEEE Trans. UFFC, vol. 33, pp. 257-264, 1986.

[14] M. Diament and M. Malekzadeh, "Ultrasound and Diagnosis of Renal and Ureteral Calculi," J Pediatr, vol. 109, pp. 980-983, 1986.

[15] C. Sehgal, et al., "Ultrasound Transmission and Reflection Computerized Tomography for Imaging Bones and Adjoining Soft Tissues," in IEEE Ultrason Symp, Chicago, IL, 1988, pp. 849-852.

[16] J. R. Jago and T. A. Whittingham, "Experimental Studies in Transmission Ultrasound Computed Tomography," Physics in Medicine and Biology, vol. 36, pp. 1515-1527, 1991.

[17] R. N. Bracewell, Two-Dimensional Imaging. Englewood Cliffs, NJ: Prentice Hall, 1995.

[18] R. N. Bracewell, Fourier Analysis and Imaging. New York: Kluwer Academic/ Plenum Publishers, 2003.

[19] M. Fox, et al., "SHARP: Sonographic Histology by Axial Rotation of Projections," in 11th New England Doppler Conference, 2004.

[20] R. Lewis, Practical Digital Image Processing. London: Ellis Horwood, 1990.

[21] E. Sirois, Chiu, D., Fox, M., Sun, W., "Aortic Root Inflation Testing Utilizing the Supercompounding Algorithm for Ultrasonic Images," in Proc. of Biomedical Engineering Society, St. Louis, 2008.

[22] S. Contreras, "Compounding and Hexagonal Filtering for Ultrasound Enhancement," Ph.D., Biomdeical Engineering, University of Connecticut, Storrs, 2011.

[23] J. Nebeker and T. R. Nelson, "Enhancement of compounded ultrasound images with spatial filtering," in Proc. SPIE 7265-34, Orlando, FL, 2009.

[24] T. Chiu, et al., "Sharpening Ultrasonography by Compounding and Deconvolution," in Proc. of 34th NEBEC, Brown University, 2008.

[25] M. Wintermark, et al., "High-Resolution CT Imaging of Carotid Artery Atherosclerotic Plaques," American Journal of Neuroradiology, vol. 29, pp. 875-882, 2008.

IntechOpen